

# END-TO-END BEAM DYNAMICS SIMULATIONS FOR THE ANL RIA DRIVER LINAC\*

P.N. Ostroumov<sup>#</sup>, Physics Division, ANL, 9700 S. Cass Avenue, Argonne, IL, 60439

## Abstract

The proposed Rare Isotope Accelerator (RIA) Facility consists of a superconducting (SC) 1.4 GV driver linac capable of producing 400 kW beams of any ion from hydrogen to uranium. The driver is configured as an array of ~390 SC cavities, each with independently controllable rf phase. For the end-to-end beam dynamics design and simulation we use a dedicated code, TRACK [1]. The code integrates ion motion through the three-dimensional fields of all elements of the driver linac beginning from the exit of the electron cyclotron resonance (ECR) ion source to the production targets. TRACK has been parallelized and is able to track large numbers of particles in randomly seeded accelerators with misalignments and a comprehensive set of errors.

## INTRODUCTION

A detailed configuration of the 1.4-GV RIA driver linac was described in ref. [2]. The linac consists of a front-end and three sections of SC linac: low-, medium- and high- $\beta$  sections. The front-end includes an ECR ion source, a Low Energy Beam Transport (LEBT) system, a Multi-Harmonic Buncher (MHB), a Radio Frequency Quadrupole (RFQ) and a Medium Energy Beam Transport (MEBT) system. The three sections of the linac are each separated by two stripper areas with a stripper foil or film and a post-stripper Magnetic Transport System (MTS). Beam dynamics in the driver linac are the most challenging for the multiple-charge-state uranium beam [2]. The baseline design of the driver linac has been optimized for simultaneous acceleration of two charge states ( $28^+$  and  $29^+$ ) in the front-end and the first section of the linac up to the first stripper and optimized for five charge states between the two strippers (average charge state is  $74^+$ ) and five charge states in the high- $\beta$  section (average charge state is  $88^+$ ). The acceleration of multi- $q$  beams not only increases the total intensity but also reduces significantly the power to dump at the strippers. For example, the five charge states after the second stripper represent 98% of the total intensity. The linac lattice is optimized for multiple-charge-state uranium beams and includes 220 SC drift tube based resonators between the front end and the second stripper. The stripping energies for uranium beam, 12 MeV/u and 89.86 MeV/u, are optimized to minimize the longitudinal effective emittance of multi- $q$  beams at the location of the strippers. The baseline design includes 172 SC cavities of elliptical type beyond the second stripper. The most recent parameters of the RIA driver baseline design were

reported in the RIA R&D workshop [3].

With cw operation of the driver linac, the space charge effects are negligible in all accelerator sections except the ECR source, the ECR extraction optics and the LEBT. The required beam intensity in the LEBT is  $500 \mu\text{A}$  for protons and  $250 \mu\text{A}$  for uranium to produce 400 kW accelerated cw beams. After separation and selection of ion species the beam optics become emittance dominated and the space charge effects produce small perturbations with respect to the “zero-current” beam optics. Downstream of the LEBT the space charge effects are negligible.

## FRONT END

### ECR-LEBT

Detailed design, optimization and simulation of the front-end is extremely important to produce a realistic beam distribution in the six-dimensional phase space at the entrance of the SC linac. Several publications have been devoted to this problem [4-6].

Beam parameters at the entrance of the LEBT have been obtained from simulations of multi-component ion beams through extraction and acceleration system of the ECR, including the extraction electrodes, solenoid lens and accelerating tube (Fig. 1). The total accelerating voltage is 100 kV. The calculations performed by the code TRACK, including static electric and magnetic field distributions and beam space charge, are consistent with the recent experimental data [7]. The achromatic section of the LEBT has been optimized to select two charge state heavy-ion beams and obtain a ~6 mm diameter beam at the location of the MHB. Figure 2 shows transverse phase space plots of dual charge state ion beam at the location of mass-analyzing slits and at the entrance of the MHB. The total extracted beam current is 3.9 mA with each charge state of  $\text{U}^{28+}$  and  $\text{U}^{29+}$  carrying 125  $\mu\text{A}$ . The simulations show that the system separates charge states reliably over full range of total input beam currents and provides at the MHB similar Twiss parameters for transverse emittances for both charge states.

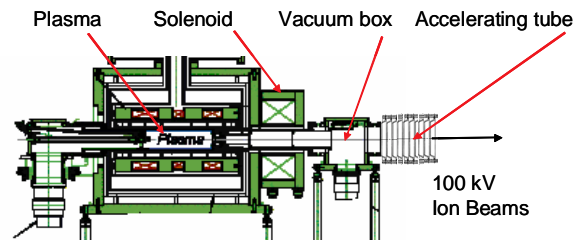


Figure 1: Beam extraction from the ECR.

Work supported by the U.S. Department of Energy, Office of Nuclear Physics, under Contract No. W-31-109-ENG-38.

<sup>#</sup>ostroumov@phy.anl.gov

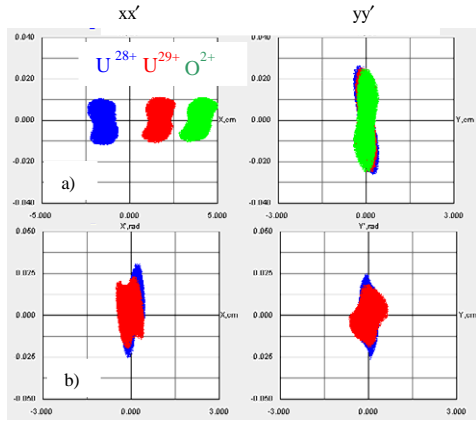


Figure 2: Beam phase space plots of a dual charge-state uranium beam at the location of the selection slits (a) and at the entrance of the MHB (b).

### MHB-RFQ-MEBT

The front-end includes different types of ion-optics devices including the MHB, RFQ and MEBT. The MEBT matches two-charge state beams to the 6D acceptance of the SRF linac. The MEBT consist of focusing elements, rebunchers, beam diagnostics tools, steering magnets and one or more choppers.

Several options for the MEBT have been studied: e.g. focusing by doublets, triplets and solenoids. It was shown that the focusing by SC solenoids is the best system for the transport of two-charge state beams. The solenoidal channel is less sensitive to the particular charge state and does not introduce additional mismatch for two-charge state beams. The beam exiting the RFQ is matched to the axial- symmetric channel by three strong electromagnet quadrupoles. The MEBT has been designed using the code TRACE3D [8] and verified by the code TRACK [1].

After the final optimization of the front-end system, the simulations including space charge of multi-component ion beams have been carried out with different numbers of particles from  $2 \cdot 10^3$  to  $10^6$ . Figure 3 shows the rms envelopes of a dual charge state uranium beam along the MHB-RFQ-MEBT section obtained from the simulation of  $10^6$  particles. Fig. 4 shows the fraction of particles  $1-N/N_0$  outside of a given longitudinal emittance. The simulation of larger numbers of particles reveals an increased beam halo. The MHB forms an extremely low longitudinal emittance of  $1.6 \pi \text{ keV/u nsec}$  containing 99% of particles. However, as is seen from Fig. 4, the total emittance for 100% of all accelerated particles which is  $8.23 \cdot 10^5$  can reach  $\sim 12 \pi \text{ keV/u nsec}$ .

The beam dynamics including space charge effects in the LEBT and RFQ has been simulated [1] and shows a 100% transmission through the RFQ including a 17.7% fraction of non-accelerated particles. The latter can be intercepted by collimators between the quadrupole lenses.

## TWO OPTIONS FOR THE LINAC

Massive parallel-computer end-to-end simulations

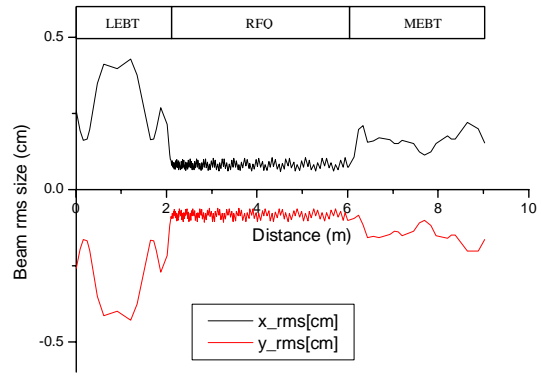


Figure 3: Two charge-state uranium rms beam size along MHB, LEBT, RFQ and MEBT. The vertical size is shown with negative sign.

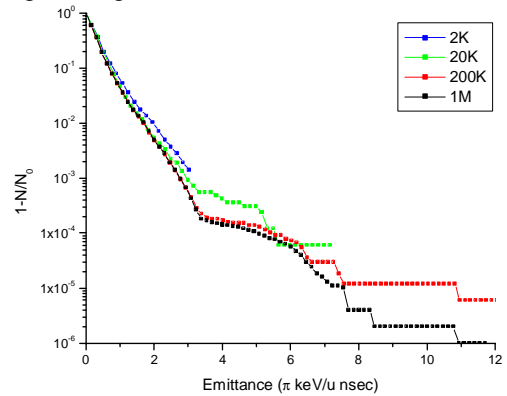


Figure 4: Fraction of particles outside of the given emittance as a function of the emittance.

have been performed for two options of the SC driver linac in order to investigate possible beam losses and determine the exact location of these eventual losses. The first option is the baseline design of the driver linac the latest update of which was described in refs. [1,3].

The second option of the driver linac is based on triple-spoke resonators (TSR) in the high- $\beta$  section of the linac [9]. In what follows we refer to the first option as the elliptical-cell linac (ECL) and the second option as the triple-spoke linac (TSL). As was mentioned in ref. [9] the obvious advantage of the TSL option is a significantly larger longitudinal acceptance compared to the ECL option. Significant cost saving in the TSL are possible primarily by reducing number of required resonators by 40 as compared to the ECL and through 4K rather than 2K operation.

Both MTSs following the strippers are provided by the set of collimators [10]. The main collimator is located in a highly dispersive area used to dump all unwanted charge states. Five other collimators are designed to clean the beam halo in the transverse phase planes. Both the ECL and TSL are designed to accept 5 charge states of uranium beam in the high- $\beta$  section, therefore only 2% of the initial intensity (about 2 kW) has to be dumped after the second stripper. The transverse acceptance of the MTS with collimators is about 10 times smaller than the acceptance of the subsequent high- $\beta$  section of the linac.

In the linac sections there are no uncontrollable mechanisms for beam halo formation, the main source of halo being the strippers. Therefore, appropriate beam collimation in the post-stripper MTS is the key solution to avoid or minimize beam losses associated with the beam dynamics.

## END-TO-END SIMULATIONS

The particle distribution exiting the front-end has been used as an initial distribution for the simulation of the SC linac. Important considerations of the accelerator "tune" include: a) beam matching between the different focusing periods; b) providing minimal beam size at the stripper location; c) transformation of the multi-q beams in the six-dimensional phase space by the MTS after the stripper; d) setting of the reference phases of the resonators to provide minimal effective emittance of the multi-q beam at the location of the strippers; e) adjustments of the collimator openings in the MTS.

Figure 5 shows the evolution of beam envelopes and emittances along the baseline linac (ECL) obtained from the simulation of 82.3% of the million particles injected into the front-end system. In these calculations, the stripper thickness fluctuation was set at 5% FWHM. After the first and second strippers 0.3% and 0.2% of particles with the accepted charge states are intercepted, respectively, by the collimators in the MTS. The sharp peaks in the beam maximum envelopes seen on Fig. 5a occur just upstream of the collimators. The controlled beam losses are mainly related to the large scattering angle and energy loss of individual particles after the stripper. The simulation without errors does not show any uncontrolled losses along the linac. Furthermore, the total transverse emittances of the beam after the MTS are defined by the set of collimators. The horizontal emittance is very similar to the vertical emittance shown in Fig. 5b. The TSL option of the linac has similar behavior for beam envelopes and emittances.

### Simulations with errors

We may classify the possible sources of error into three groups: a) Misalignment errors affecting all the elements of the accelerator system: accelerating cavities, quadrupoles, solenoids,... b) Rotation errors affecting mainly quadrupoles, multipoles and bending magnets. c) RF field errors affecting the field level as well as the phase of an accelerating cavity. For heavy ions requiring stripping another important source of error is the fluctuation in the thickness of the stripper foil or film [10]. The errors are of two types: static and dynamic. Misalignments of accelerator elements are considered as static errors. A jitter of RF and focusing fields is an example of a dynamic error. The phase and amplitude setting of the accelerating cavities when first tuning the accelerator or when restoring a tune is also a source of static errors.

Table 1 lists the errors considered as well as their typical amplitudes. We have studied the effects of

individual type of errors on beam dynamics by varying individual amplitudes through wider range than is shown in Table 1. In practice, we expect alignment within  $\pm 200 \mu\text{m}$ , as was demonstrated at TRIUMF [11]. The errors in the beam dynamics simulations are generated randomly based on appropriate distributions [1].

### Beam-based correction

The most critical errors affecting transverse beam motion of multi-q ion beams are the misalignments of transverse position of focusing elements and low-beta SC resonators. As was discussed in ref. [12] multi-q beams require corrective steering in order to avoid emittance growth. A minimization algorithm has been developed that can correct both position and angle in the four-dimensional transverse phase space. The algorithm has been fully integrated into the code TRACK. The details of the method can be found in ref. [13]. As a beam-based

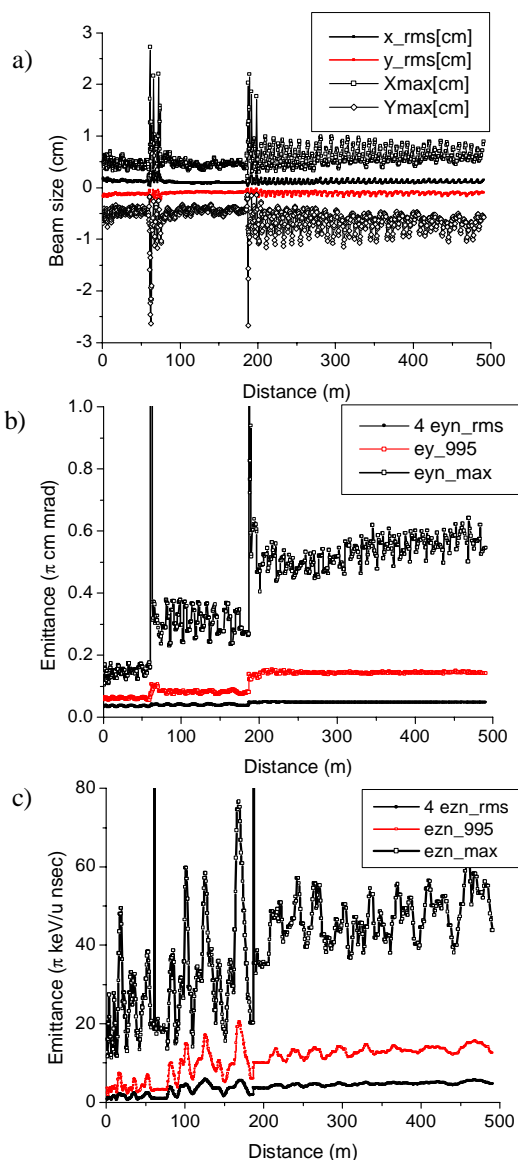


Figure 5: Beam envelope (a), transverse emittance (b) and longitudinal emittance (c) evolution along the linac.

Table 1: Sources of static errors and their typical values. For solenoid displacements, the error depends on the solenoid length.

	Description	Value
1	Cavity end displacement	0.05 cm
2	Solenoid end displacement	0.015-0.05 cm
3	Quadrupole end displacement	0.01 cm
4	Multipole rotation	2 mrad

method, one of the essential features is that it can be implemented experimentally. The beam-based steering algorithm is applied to every randomly generated accelerator seed to determine the steering correctors setting along the whole linac for the given set of the element misalignments. The final tracking of large number of particles occurs in the misaligned accelerator with corrective steering applied. To achieve effective steering for the whole linac, the latter is divided into 10-15 short sections to which the steering algorithm is applied. Figure 6 shows the beam centroid evolution along the linac. The misalignment amplitudes are taken from Table 1. Note, without corrective steering a major fraction of the beam would be lost.

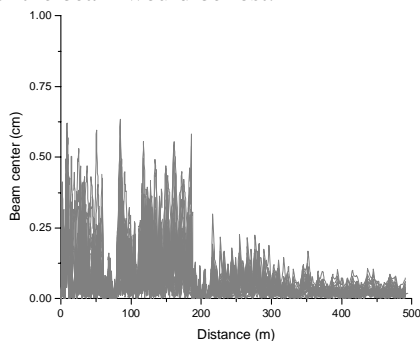


Figure 6: Multi-q beam center  $\sqrt{X_c^2 + Y_c^2}$  as a function of the distance. The figure shows trajectories of multi-q beam center along the linac for all 50 accelerator seeds.

## BEAM LOSS ANALYSIS

In this section we apply all of the errors simultaneously and study the beam dynamics and the eventual beam losses. Different combinations of amplitudes for RF errors and stripper thickness fluctuations are used as shown in Table 2. Additional errors have the same values as shown in Table I and are kept unchanged in each calculation. Both the baseline and triple-spoke designs of the accelerator were simulated using 200 sets of errors for each combination. For each set  $2 \cdot 10^5$  particles are tracked for a total of 40 million particles. Figure 7 shows particle coordinates at the exit of the accelerator for the different error combinations accumulated for all seeds. From these plots we notice that while the transverse beam size is unchanged for the triple-spoke design it is increasing for the baseline (ECL) design as is the longitudinal emittance.

This may be due to a coupling of the transverse and longitudinal motion for particles near the separatrix in

Table 2: Combinations of RF field amplitude, phase errors and foil thickness fluctuations. Uncontrolled beam losses are given for the ECL and TSL options of the driver linac.

Comb.	Rms RF errors	Thick. fluct.	ECL	TSL
1	0.3%, 0.3°	5%	$3.0 \times 10^{-8}$	0.
2	0.3%, 0.3°	10%	$8.2 \times 10^{-7}$	0.
3	0.5%, 0.5°	5%	$5.5 \times 10^{-5}$	0.
4	0.5%, 0.5°	10%	$2.7 \times 10^{-4}$	0.
5	0.7%, 0.7°	5%	$1.4 \times 10^{-3}$	0.
6	0.7%, 0.7°	10%	$2.6 \times 10^{-3}$	0.

the longitudinal phase space. Some of these particles may lose stability and eventually be lost. Table 2 shows the fraction of beam lost in the high- $\beta$  sections of the linac for the different error combinations and both accelerator designs. The values in Table 2 are the average of 200 sets for each combination of errors defined in columns 2 and 3. The baseline and triple-spoke designs have very similar low and medium energy sections therefore the  $\sim 0.3\%$  loss (in addition to the losses of unwanted charge states) in the stripper areas are similar for both designs and independent of the combination of errors. Beam losses are observed in the high- $\beta$  section for the baseline design whereas no losses are observed for the triple-spoke design. The losses seem to increase with both the RF errors and the fluctuation in the stripper thickness. The recommended values of errors for the baseline design of the driver linac should therefore be less than or equal to those listed in row 3 in Table 2. ‘Combination 4’ already produces power losses on accelerator structures higher than 1 W/m [1]. In the simulations we have not included radioactive products generated on the second stripper. However, the uncontrolled losses of radioactive ions should not exceed several units of  $10^{-6}$  according to analytical estimations.

This study clearly indicates that the current baseline design imposes more stringent error tolerances, whereas, the triple-spoke design is more tolerant of errors.

## ACKNOWLEDGEMENT

The author is grateful to the colleagues Drs. V.N. Aseev, A.A. Kolomiets, E.S. Lessner, B. Mustapha, J.A. Nolen, R.C. Pardo, K.W. Shepard, T. Wangler who made possible the extensive beam dynamics studies in the driver linac by their significant contributions and stimulating discussions.

## REFERENCES

- [1] P.N. Ostroumov, V.N. Aseev, and B. Mustapha. Beam loss studies in high-intensity heavy-ion linacs, Accepted for publication in PRST-AB, June 9, 2004.

- [2] P.N. Ostroumov, Phys. Rev. ST Accel. Beams 5 (2002) 030101.
- [3] K. Shepard, RIA R&D Workshop, Washington, D.C., August 26-28, 2003, paper 2.2.3.
- [4] P.N. Ostroumov, et al., Proc. of the LINAC'2000, Monterey, CA, p. 202.
- [5] P.N. Ostroumov, et al., Phys. Rev. ST Accel. Beams 5 (2002) 060101.
- [6] A.A. Kolomiets et al., Proc. of the PAC-2003, Portland, OR, p. 2875.
- [7] D. Leitner, ECR Ion sources for RIA, RIA Facility Workshop, March 9-13, 2004, [http://meetings.nsl.msui.edu/ria2004/talks\\_dl.php](http://meetings.nsl.msui.edu/ria2004/talks_dl.php).
- [8] K.R. Crandall, TRACE 3-D Documentation, Report LA-11054-MS, Los Alamos, 1987.
- [9] K.W. Shepard, P. N. Ostroumov, and J. R. Delayen, Phys. Rev. ST Accel. Beams 6 (2003) 080101.
- [10] P.N. Ostroumov, in Proceedings of the 29th ICFA Advanced Beam Dynamic Workshop, Montauk, New York, 2003, AIP Conf. Proceedings, 693, p. 53.
- [11] B. Rawsley, et al. A Wire Position Monitor Alignment System for the ISAC-II Cryomodule Components Alignment. Paper MOP89 in this proceedings.
- [12] P.N. Ostroumov and K. W. Shepard, Phys. Rev. ST Accel. Beams 3, 030101 (2000).
- [13] E.S. Lessner and P.N. Ostroumov, Proc. of the EPAC'04, Lucerne, Switzerland, paper TUPLT147.

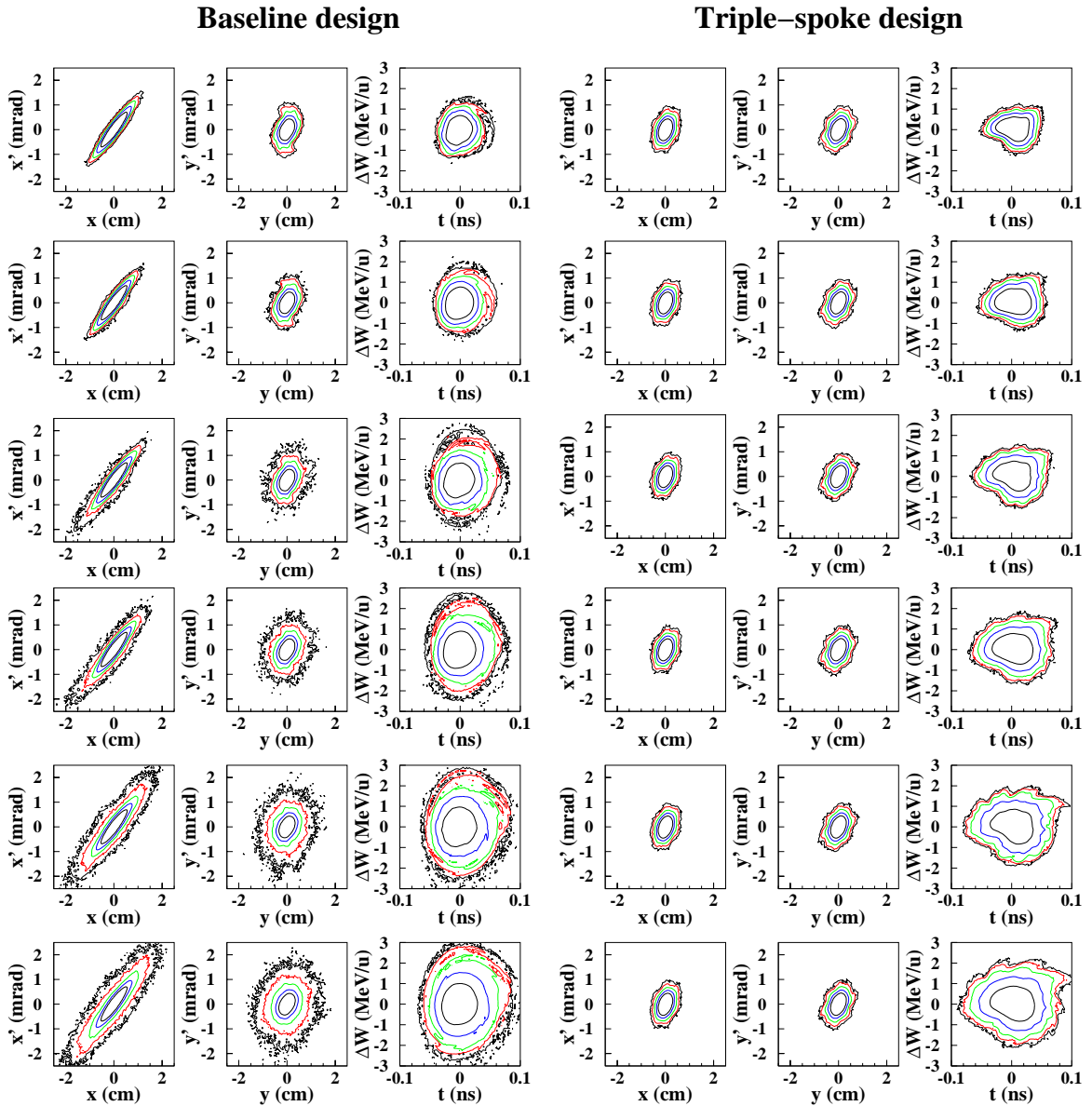


Figure 7: Phase space plots for the both accelerator designs and error combinations of table II. The six rows here correspond to the six rows in Table 2. The logarithmic density isolines are represented by different color.